Metadynamics Simulations for Rational Ligand Design in the Reversible Inhibition of Human Peroxiredoxin 5

Laura Troussicot [1,2,✉], Florian E.C. Blanc [1], Yoann Pascal[3], Sebastien Vidal [3,4], Jean-Marc Lancelin[1,*], and Florence Guillière [1]

[1]Institut des Sciences Analytiques UMR 5280, CNRS, Universite Lyon 1, Universite de Lyon, 5 rue de la Doua, F-69100 Villeurbanne, France
[2]MMSB Lyon, UMR5086 CNRS Lyon University, 7, passage du Vercors, 69367 Lyon Cedex 07, France
[3]Institut de Chimie et Biochimie Moléculaires et Supramoléculaires, UMR 5246, CNRS, Université Claude Bernard Lyon 1, Université de Lyon, INSA Lyon, CPE Lyon, Villeurbanne, 69622, France
[4]Institut de Chimie des Substances Naturelles, UPR 2301, CNRS, Université Paris-Saclay, Gif-sur-Yvette, 91198, France
[*]Presently retired

Based on Funnel-Metadynamics, a molecular dynamics protocol that provides an accurate representation of protein-ligand interaction, the activity of an initial hit of Human peroxiredoxin 5 was improved by several orders of magnitude by the introduction of a single heavy-atom modification. This improvement was followed by molecular dynamics simulation and NMR experiments with striking agreement. We demonstrate that molecular dynamics is a rational basis for the design of straightforward improved ligands starting from low-affinity but selective hits with a minimum adaptation. This result can only be reached by analyzing the statistical quantitative description of the protein-ligand interactions available through molecular dynamics simulations.

Molecular Dynamics| Ligand Design | NMR | Enzyme Inhibition | Funnel metadynamics

Correspondence: ***laura.troussicot@cnrs.fr***

Introduction

The design of ligands to modulate the activity of biological receptors is central to drug discovery (1, 2). In fragment-based approaches, low-affinity but selective simple molecules are optimized through chemical modifications until they bind to the target with maximum lasting efficiency (3, 4). In this study, we highlight how quantitative-accuracy Molecular Dynamics simulations can enable the rational design of an improved inhibitor against an enzyme relevant for Human health.

The thermodynamics of ligand-receptor binding can be studied at the macroscopic level by *in vitro* biophysical methods (e.g., NMR, enzyme kinetics) or computationally by Molecular Dynamics (MD) simulations. A key interest of MD is that it provides atomically detailed insight into the drug-target interaction. However, quantitative prediction of binding affinity by simulations remains challenging and requires computationally costly free energy calculation techniques (5–10). Among them, alchemical methods evaluate the free energy difference along artificial transformations in which the protein/ligand interactions are progressively turned on (or off) (11). These methods can accurately predict the binding affinity, but their non-physical character makes it challenging to infer mechanistic information. Alternatively, geometric methods evaluate the binding affinity by collecting the change in free energy along geometric degrees of freedom that describe the binding process, such as the distance between the ligand and the binding site (12). This can provide more realistic molecular details than in the alchemical case. However, reaching convergence requires specialized protocols to control the translational, rotational, and conformational entropy of the ligand. Funnel metadynamics (FM) combines metadynamics, a popular geometrical free energy method (13, 14), with a funnel-shaped restraining potential to focus the sampling on reversible binding events (15). This promotes the convergence of the binding free energy estimate. A few years ago, we highlighted the potential of FM for drug design by demonstrating how it can quantitatively predict binding affinities of enzymatic inhibitors (16). Since then, FM has been widely used for elucidating ligand binding modes of several biological systems. (17–20). The connection between the microscopic and macroscopic descriptions of binding provided by the free energy landscape offers a powerful way to engineer the affinity of ligands against a known receptor, rationalizing the optimization process. Here, we apply FM to the design and validation of an inhibitor of Human peroxiredoxin 5.

Human peroxiredoxin 5 (hPrx5) is a thiol-active peroxidase that catalyzes the decomposition of hydroperoxides, and is part of the peroxiredoxin superfamily (21, 22). Peroxiredoxins are involved in many cellular processes (23, 24) and were recently identified as key initiators of post-ischemic inflammation (25). hPrx5 therefore emerges as a target for the development of treatments against strokes, and has been the object of screening campaigns. Notably, we previously screened hPrx5 by NMR and discovered fragment molecules from the catechol family as active-site ligands and potential inhibitors (26). Later on, we described their binding/unbinding to hPrx5 using unbiased MD and FM, achieving a free-energy prediction that matched quantitatively the low affinity determined by high-accuracy solution NMR (16). Further, we correlated the binding affinities of catechol, 4-methylcatechol (4MEC) and 4-tert-butylcatechol (4TBC) to hPrx5 to a reversible inhibition mechanism using steady-state kinetics, demonstrating a partial mixed-type non-competitive mechanism, in agreement with FM simulations in the pres-

DRAFT

ence of the substrate (27).

In these previous studies, the simulations indicated that the rather rigid ligands (CAT, 4MEC, 4TBC) could adopt several bound state conformations (three conformations bound to the catalytic cysteine via one or two hydrogen bonds, as well as a conformation bound to the Glu179 side-chain in the active site cavity), and that the fluctuation of the active-site geometry was affected during the binding periods (27). Whereas 4MEC binding caused, on average, a reduction in the volume of the active site (16), 4TBC caused a significant global expansion during the binding periods as seen in Fig S1 around $300\,\mathrm{ns}$ of simulation (full analysis also shown in SI). From these observations, we hypothesized that the introduction of an additional degree of freedom in the substituent of catechol should lead to an improved affinity and inhibition. Indeed, we reasoned that it would help the ligand better adapt to the active-site dynamics, and hence reduce the conformational dispersion during the binding periods by stabilizing a binding mode relative to the others. Through simulations and experiments, we show here that this is in fact the case: an additional degree of freedom in the ligand structure — lengthening the aliphatic tail by one carbon atom to obtain the corresponding 4-neo-pentylcatechol (4NPC) — improves the inhibition of hPrx5 by several orders of magnitude.

Results

Funnel Metadynamics predicts improved binding affinity of 4NPC for hPrx5. To test our hypothesis, we performed careful free energy simulations with the Funnel Metadynamics (FM) method to assess whether 4NPC does exhibit an improved affinity for hPrx5. In a $1\,\mu\mathrm{s}$ FM simulation with 4NPC, we observed 6 binding events of various durations, the longest being $\approx 100\,\mathrm{ns}$ (see S1 and S2). This observation, along with the stabilization of the free energy estimate in the second half of the simulation, strongly supports the proper convergence of this challenging calculation. This allows us to evaluate the absolute binding free energy ΔG_b^0 (from the free-solvated state to the bound form) at the convergence of the calculation (15).

The estimated $\Delta G_b^o = -6.2 \pm 0.5\,\mathrm{kcal\,mol^{-1}}$ found by FM predicts a significantly improved affinity in comparison with all previous catechol derivatives (Table 1) (16, 27). Thus, FM provides us with a quantitative estimation of the affinity of the complex, which encouragingly predicts that the proposed derivative should indeed exhibit improved affinity towards the target. Next, to unravel the atomistic determinants of improved binding, we analyze the FM trajectory and compare it to previous simulations of other hPrx5 binders.

Ligand dynamics within the active site. We analyzed the trajectory to get insight into the conformational dynamics of ligands in the active site, and how it can be related to affinity differences. For this purpose, we first projected the 4NPC FM trajectory onto three collective variables (CVs). CV1 is the ligand-active site distance, that is, the one biased in the FM calculation. CV2 and CV3 are designed to capture the conformational state of the ligand (CV2) and its orientation relative to the active site (CV3); see Methods section for more information on CVs. Thus, our protocol provides direct insight into how binding to the protein shapes the conformational landscape of the ligand. Using a rigorous reweighting procedure with PLUMED ((28, 29)), we mapped the free energy as a function of CV1 and CV3. The analysis of this free energy landscape depicted in Fig. 1 reveals three local free energy minima in the bound state. Structural clustering shows that these correspond to four major binding conformations A, B, C and D. Three of them (A,B,C) interact directly through H-bonding with the catalytic thiolate of Cys47 while the neopentyl group is in Van der Waals lateral contacts to the hPrx5 active site region including Leu116, Ile119 and Phe120 (1). The fourth cluster (D) retains these lateral interactions while making stabilizing polar interactions with Glu179 at the surface of hPrx5, as previously detected for 4TBC (27), and is $1\,\mathrm{kcal\,mol^{-1}}$ higher in free energy. Overall, in comparison with previous catechol fragments, only four different conformers are detected, all within $1\,\mathrm{kcal\,mol^{-1}}$ of one another and separated by low ($\approx 2\,\mathrm{kcal\,mol^{-1}}$) barriers, suggesting that they exchange rapidly and all contribute to the bound state. Moreover, we observe that 4NPC does not induce significant changes into the active site fluctuations, as depicted in the lower panels of Fig. S1. This suggests that 4NPC exhibits better flexibility and adaptation to the active site geometry, allowing longer binding periods.

NMR assay confirms the predicted affinity of 4NPC for hPrx5. We measured the affinity of 4NPC for hPrx5 by solution NMR assays (2). The ^{1}H-^{15}N chemical shift perturbations (CSP) observed on ^{1}H-^{15}N-HSQC spectra in the presence of the 4NPC were successfully fitted to a simple binding model (see Methods), allowing us to estimate the binding affinity. We found an NMR-based average dissociation constant $K_D = 20 \pm 10\,\mu\mathrm{M}$; remarkably, this value falls within the statistical fluctuations of the FM prediction. Furthermore, the CSPs exhibited greater magnitude compared to those observed with other catechol fragments (Fig. S3), likely indicating less dispersed bound conformations. A comparison of the CSPs induced in the case of 4TBC and 4NPC reveals that the enhancement in affinity is accompanied by a greater degree of disruption of the Leu116-Phe120 hydrophobic helix, as well as the residues located in the vicinity of Cys47. This increase in the CSPs reflects the enhanced stability of the bound form of the PL complex. Finally, an NMR saturation transfer difference (STD) epitope mapping (Fig. 2) reveals that protons H5 and H6 exhibit a much larger degree of saturation transfer (respectively 90% and 100%) than proton H3, suggesting that H5 and H6 are burried into the protein-ligand interface whereas H3 is more solvent-accessible. These characteristics are consistent with the ligand poses observed in clusters A and B (Fig 1), which were predicted as dominant from the FM simulations. Therefore, NMR measurements quantitatively confirm the simulation-based affinity prediction and also recapitulate the ligand/receptor conformational landscape observed in the simulation.

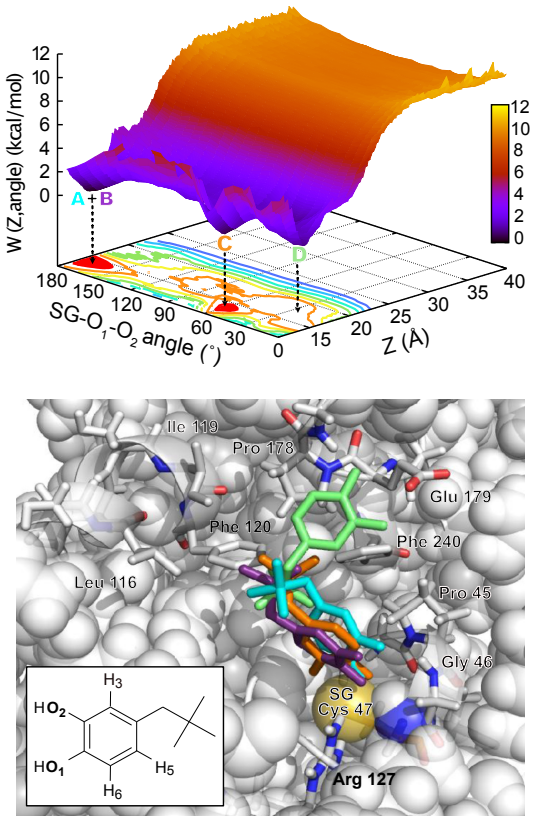

Fig. 1. Free-energy surface (FES) and geometry of the 4NPC-hPrx5 interaction. Upper panel: FES as a function of two collective variables used in FM calculations. CV1: projection on the Z axis of the distance between Cys47 SG and the center of mass of the ligand heavy atoms (Å) and CV3: SG-O1-O2 angle (deg) between sulphur atom of the catalytic cysteine and oxygen atoms of the diol ligand. Iso-energy contours are drawn using $1\,\mathrm{kcal\,mol^{-1}}$ interval. Lower panel: visualisation of the four bound conformations obtained after geometrical clustering of the FM trajectory with a $2\,\mathrm{\AA}$ cutoff, representative of the three free-energy basins A+B, C and D. Cys47 is shown as a yellow Van der Waals sphere and clusters conformations are colored as follows: A: blue , B: purple, C: orange, D: green.

Inhibition mechanism and enzymology. Next, we set out to find out whether the increasing binding affinity actually translates into an improved inhibitory effect as compared to previously characterized catechol derivatives. For this purpose, we conducted experiments to evaluate the reversible mechanism of inhibition for 4NPC, and compared it to other catechol fragments (27). First, our enzymatic assay yielded an IC50 of $40 \pm 5\,\mu\mathrm{M}$ (SI section S4) for 4NPC, considerably lower than for catechol ($3730 \pm 850\,\mu\mathrm{M}$) and the tert-butyl derivative ($250 \pm 60\,\mu\mathrm{M}$), see Table 1. Then, we studied the mechanism of inhibition using steady-state kinetics analyzed with non-linear regression models (30, 31). Reaction rates were fitted against the concentration of H_2O_2 for each concentration of 4NPC and found to fit best with a partial mixed non competitive inhibition model. In this model, 4NPC can either bind to the reduced-free enzyme and to the Enzyme-Substrate (ES) complex (Fig. S5) with two different affinities (K_i and K_i'). Based on the values obtained for inhibition constants (K_i and K_i') and catalytic rates (k_{cat} and k_{cat}') given in Table 1, 4NPC binds preferentially to the free reduced enzyme ($K_i < K_i'$) and the ternary ESI complex is inhibited ($k_{cat} > k_{cat}'$). The inhibition constants (K_i) indicate that 4NPC inhibits the free reduced hPrx5 100 times better than catechol, and 5 times better than 4TBC, demonstrating that we have obtained an improved inhibitor through rational modifications.

	Catechol	4TBC	4NPC
Affinities			
$\Delta G_b°$(kcal.mol^{-1})^c	-3.0 ±0.2^a	-5.5 ±0.9^b	-6.2 ±0.1
K_D (µM) - FM^c	6900 ±2100^a	110 ±90^b	60 ±30
K_D (µM) - NMR^c	4500 ±600^a	190 ±30^b	20 ±10
Inhibitions			
IC50 (µM)	3730 ±850	250 ±60	40 ±5
K_M (µM)	40.7 ±4.0^b	36.9 ±4.4^b	26 ±2
Ki (µM)	1810 ±460^b	90 ±40^b	19 ±5
Ki' (µM)	4040 ±1130^b	180 ±100^b	80 ±40
k_{cat} (s^{-1})	3.08 ±0.08^b	3.05 ±0.1^b	2.15 ±0.05
$k_{cat'}$ (s^{-1})	∼ 0^b	2.35 ±0.18^b	0-0.67^d

[a] Data from a previous report. (16); [b] Data from a previous report. (27); [c] In FM, $\Delta G_b°$and K_D were calculated by standard deviation, reweighted over the simulation time (last 100 ns over 500 ns for catechol and 4TBC, and last 400 ns over 1000 ns for 4NPC). In NMR K_D was calculated from CSPs.; [d] $k_{cat'}$ was determined inaccurately with an upper limit of 0.67 s^{-1}.

Table 1. Comparison of the predicted and the experimentally determined affinities and inhibitions of catechol derivatives against hPrx5

Discussion and Conclusion

Protein-ligand affinity results from a complex interplay between strong interactions and conformational plasticity. Small, rigid ligands tend to favor strong binding by reducing entropic penalty, but the affinity gain can be offset if the ligand is too rigid to interact optimally with the binding site. Here, we improved the affinity of an inhibitor by tuning intermolecular interactions and flexibility to promote conformational adaptation to the target active site (Fig. 3). The introduction of one degree of freedom in 4NPC leads to a better flexibility of the ligand, an increase in conformational exploration and thus a better adaptation to the active site through the formation of additional intermolecular interactions besides the binding to the catalytic cystein. It also stabilizes the main binding mode, leading to longer binding periods instead of conformational exchange. We introduced what is arguably the simplest, minimum structural modification to that effect. This leaves a lot of unexplored chemical space to evolve toward a drug-like compound with further improved, nanomolar inhibitory properties against hPrx5. We expect the insights into protein-ligand interactions afforded by FM to be precious for this next optimization step.

Methods

Protein expression and purification. Recombinant human Prx5, yeast Trx, and yeast TrxR were in the pQE-30 expression vector (Qiagen) with an N-terminal fusion with hexahistidine (6xHis) tag. The expression and purification of the

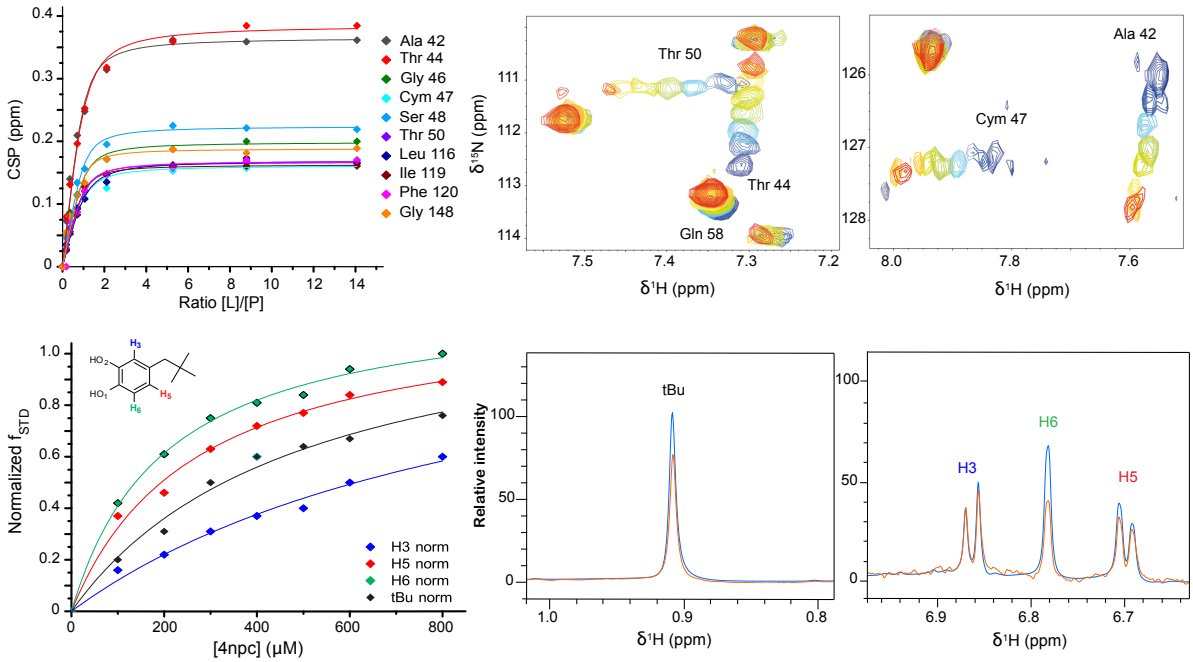

Fig. 2. Affinity assay of 4NPC for hPrx5 using NMR. Upper panels: plot of the NMR CSP obtained as a function of ligand-to-protein concentration ratio, and two partial overlays of ^{1}H-^{15}N HSQC spectra of hPrx5 with various concentrations of 4NPC in PBS pH=7.4 at $301\,\mathrm{K}$, from blue (hPrx5 only) to red (saturation of the binding site by 4NPC). Lower panels: plot of the STD factor against ligand concentration for aromatic protons and tert-butyl group, and spectral overlays of the 1D spectra (blue) and the STD spectra (orange) obtained for [4NPC] = 0.8mM.

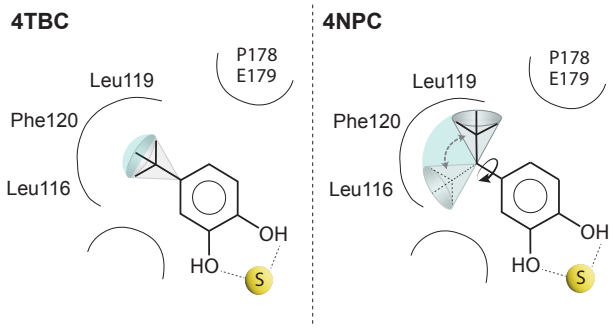

Fig. 3. Chemical modification to tert-butyl-catechol led to improved spatial adaptation.

proteins were adapted from Declercq et al. 2001 (32). The plasmids kindly provided by Dr. Bernard Knoop's lab (Université Catholique de Louvain, Belgium) were transformed into *Escherichia coli* strain M15 (pRep4) and grown in LB medium at 37°C. To produce ^{15}N labeled human hPrx5, cells were expressed in M9 minimal medium (6 g/L Na_2HPO_4, 3 g/L KH_2PO_4, 0.5 g/L NaCl) supplemented with 6 µg/L thiamine, 1 mM $MgSO_4$, 1 mM $CaCl_2$, 10 mL/L trace metal solution, 4 g/L glucose, two resistance antibiotics (kanamycin and ampicillin 50 µg/mL) and containing 1 g/L $^{15}NH_4Cl$ as the sole nitrogen source. The bacterial cultures were induced for an O.D. of 0.6 with 1 mM of isopropyl β-D-1-thiogalactopyranoside (IPTG) for 4 to 5 hours and were then centrifuged for 20 min at 3000 rpm. The resulting bacterial cell pellets were lysed by sonication using a solution containing 10 mM imidazole, 50 mM phosphate and 300 mM NaCl pH 8 (lysis buffer). The cell lysate was then centrifuged for 45 min at 12000 rpm and the supernatant loaded into a Ni^{2+}-NTA column (Qiagen). The column was washed with lysis buffer and the protein was eluted with 250 mM imidazole, 50 mM phosphate, 300 mM NaCl pH 8. The eluted protein was pooled and dialyzed overnight against PBS pH 7.4 at 4°C, then analyzed by SDS-PAGE. Its final concentration was quantified by UV-Vis spectrum (A280: Trx (ε = 10095 M^{-1} cm^{-1}), TrxR (ε = 24660 $M^{-}1$ cm^{-1}), and human Prx5 (ε = 5625 M^{-1} cm^{-1}) with ε calculated from Expasy website (expasy.org/protparam).

Molecular Dynamics Simulation. MD systems were prepared, minimized, and equilibrated as described previously (16) from the high-resolution crystal structure of homodimeric hPrx5 (PDB entry: 3MNG) (33, 34). Crystallographic water molecules were retained and added to the protein coordinates. Hydrogen peroxide and ligands were positioned manually near one of the two active sites of the homodimer, and the catalytic cysteine (Cys47) was modeled as a thiolate. Finally, Na^{+} and Cl^{-} were added to match 150 mM sodium chloride aqueous solution, close to the experimental conditions used, and neutralize the total charge of the system. Simulations were performed with the AMBER99SB-ILDN force field (35–37) for the protein, and the TIP3P water model for the explicit solvent (38). Amber charges were applied to protein, substrate, ligands, ions, and water atoms, in addition to the restrained electrostatic potential charges which were used

for the ligands using the Antechamber program suite (39) and the General Amber Force Field (GAFF) (40). The system was minimized and equilibrated under constant pressure and temperature (NPT) conditions at 1 atm and 300 K using ACEMD as described in reference (6), and the PLUMED plugin was used to carry out funnel-metadynamics calculations (29). Since the funnel external potential was fixed in the space, diffusion of the whole protein was canceled by harmonically restraining the positions of 3 atoms chosen far from the interface of the homodimer or from the active site, namely the Cα atoms of G6, G31, and K65 of chain A with a force constant of $20\,\mathrm{kcal/mol/Å}^2$ in ACEMD. We evaluated the free energy profile along the distance of the ligand to the center of the active site by well-tempered metadynamics in presence of the funnel potential. Three collective variables (CV) were defined : the projection on the Z-axis of the distance between Cys47 SG and the center of mass of the ligand heavy atoms (CV1), the distance from the funnel Z-axis of the ligand center of mass (CV2) and the protein-ligand torsion angle Cys47 SG...O1-C1-C2 (ligand). The bias was applied on CV1, and the values of all CVs were collected along the simulations to evaluate the conformational space explored by the system. A Gaussian width of 0.35 Å and deposition rate of $0.25\,\mathrm{kcal\,mol^{-1}\,ps^{-1}}$ (1 kcal = 4.18 kJ) were initially used and gradually adapted using well-tempered metadynamics (7). At convergence, the binding free energy was recovered from the Potential Mean Force after correcting for the entropic penalty of the funnel. Trajectories were analyzed using VMD (41). Geometric clustering of bound ligand conformations was performed with a Quality Threshold approach (42) implemented in VMD Clustering V 2.0 (Luis Garcia, Cornell Medical College, USA) with a 2 Å RMSD cutoff.

Chemical Synthesis of the 4-neopentylbenzene-1,2-diol or 4-neopentylcatechol (4NPC). The 4-neopentylbenzene-1,2-diol **4** was synthesized from 1,2-dimethoxybenzene **1** according to the scheme depicted in Fig. 4. The Friedel-Crafts acylation was performed in an ionic liquid (43) with $Bi(OTf)_3$ and the resulting t-butylphenylketone **2** was reduced to the corresponding alkane **3** under green conditions (cyclopentyl methyl ether - CPME) and Pd/C 5% as catalyst (44). The final removal of the methyl ethers with BBr_3 provided pure 4NPC product **4** as a white crystalline powder. The details of the synthesis steps are available in SI, as well as the mass spectrometry and NMR analysis of the different intermediates, and the corresponding ^{1}H and ^{13}C NMR spectra (Fig. S7, S8 and S9).

Solution NMR experiments. HSQC experiments were monitored at 28 °C with a Varian Inova 600 MHz MHz NMR spectrometer equipped with a 5 mm standard triple resonance (^{1}H/^{13}C/^{15}N) inverse probe with a z-axis field gradient. STD standard 1D and STD experiments were performed on the same Varian Inova 600 MHz NMR spectrometer further equipped with a 5 mm PFG triple resonance HCN cold probe at 28 °C. NMR pulse sequences used for those

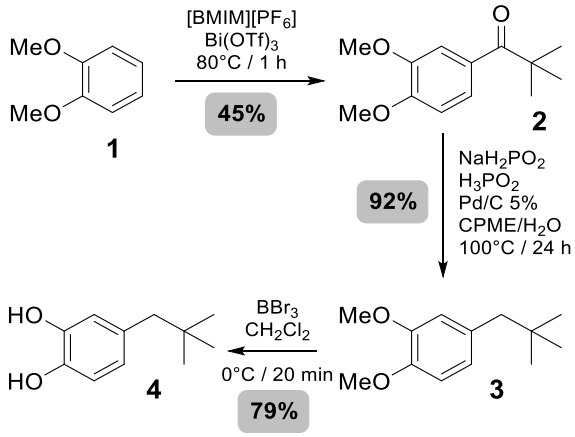

Fig. 4. Scheme: Chemical synthesis of 4-neopentylbenzene-1,2-diol (4NPC) and the yields obtained for the different steps of the synthesis.

experiments were taken from the Agilent Biopack ensemble of experimental schemes within Agilent VnmrJ 4.2 software. For HSQC experiments, a Watergate water suppression HSQC sequence and for STD experiment a Saturation Transfer 1D sequence were chosen. The binding interaction of 4NPC to hPrx5 was characterized through a series of two-dimensional ^{1}H-^{15}N-HSQC NMR experiments. NMR samples contained 200 µM of the reduced ^{15}N-labeled protein, kept in its reduced form by addition of 2 mM of tris(2-carboxyéthyl)phosphine (TCEP), in phosphate buffer saline (PBS) pH 7.4. An increasing concentration of 4NPC previously dissolved in dimethyl sulfoxide (DMSO) was added until binding saturation was reached. DMSO's influence on chemical shift was tested until 8%. All spectra were processed using NMRPipe/NMDraw package (45) and ^{1}H-^{15}N chemical shift perturbations (CSPs) were assigned using NMRViewJ software (46). The combined amide CSPs $\Delta\delta$ were calculated according to the following expression:

$$\Delta\delta = \sqrt{\frac{\Delta\delta_H^2 + (\frac{\Delta\delta_N}{5})^2}{2}}$$

Upon characterizing the amide CSP $\Delta\delta$ to the specific amino acid residues involved in the binding interactions, a binding dissociation constant (K_D) was extrapolated from the curve plotting the CSP values versus the concentration ratio [Ligand]/[hPrx5] as previously described by Lange et al. 2011 (47). The binding of 4NPC to hPrx5 was also investigated using ^{1}H Saturation Transfer Difference (STD) NMR spectroscopy. NMR samples were prepared in PBS (pH 7.4) with 10 µM hPrx5 in presence of TCEP (500 µM) to keep it in reduced form, and 4NPC was added from 100 µM to 1 mM. 1D and Saturation Transfer Difference (STD) experiments were acquired using identical conditions, and all STD spectra were recorded with the same parameters (saturation

period = $2.0\,\mathrm{s}$, made of 40 Gaussian pulses of $50\,\mathrm{ms}$). The number of scans was set to 512 for 1D spectra and 1024 for STD, and the selective irradiation of the protein was performed at the decoupler offset of $-3006\,\mathrm{Hz}$ downfield from the carrier frequency (-0.23 ppm) and off-resonance control was performed at $15\,000\,\mathrm{Hz}$ upfield. STD signals were then measured for aromatic protons and tert-butyl group, and the STD factor was calculated and then normalized by setting the largest value, following the formula:

$$f_{STD} = \frac{I_{STD}}{I_{1D}} \cdot \frac{[\text{4NPC}]}{[\text{hPrx5}]}$$

where f_{STD} is the STD factor, I_{STD} is the integral of a given STD signal, I_{1D} is the integral of the normal spectrum of the same signal, and $[\text{4NPC}]/[\text{hPrx5}]$ is the ligand to protein concentration ratio.

Half Maximal Inhibitory Concentration Assay (IC50). The inhibitory concentration assay of hPrx5 was carried out as described by Chow et al. 2016 (27). The inhibition activity of hPrx5 with 4NPC was indirectly measured by the coupling reaction of thioredoxin reductase (TrxR) oxidizing Nicotinamide Adenine Dinucleotide Phosphate (NADP) monitored with the absorbance of NADPH at $340\,\mathrm{nm}$ (A^{340})(Fig.S4). Within a total of 1000 µL, the reaction solution consists of 4NPC at 0–5000 µM range, 15 µM of yeast thioredoxin (Trx), 2 µM of yeast TrxR, 0.15 µM of human Prx5, 200 µM of NADPH and 25 µM of H_2O_2. The reaction was carried out by a mixture of all three proteins diluted in PBS containing $1\,\mathrm{mM}$ of ethylenediamine tetraacetic acid (EDTA) pH 7.0 and the successive addition of 4NPC and NADPH. Lastly, H_2O_2 was added to the mixture and mixed well to initiate the inhibition activity of hPrx5 at room temperature. The reaction was monitored at A^{340} for 200 seconds on a Jasco UV-Visible spectrometer, and the initial rate of the reaction was determined from the linear portion of the curve and is expressed in $\mu\mathrm{mol\,min^{-1}\,mg^{-1}}$ of hPrx5.

Inhibition mechanism assay . Assays to determine the inhibition mechanism of 4NPC for human hPrx5 were adapted from Chow et al. 2016 (27). 4 different concentrations of 4NPC were used, taken above and below the value of IC50 (40 ± 5 µM). The reaction was carried out by mixing together hPrx5 (0.15 µM), yTrx (15 µM), yTrxR (2 µM), 4NPC, and NADPH (200 µM) (S5). The reaction was started with the addition of H_2O_2 (ranging from 0 to 500 µM) in the reaction mixture. The reaction was monitored with the same device and parameters as for the IC50 determination, and the rate expressed in $\mu\mathrm{mol\,min^{-1}\,L^{-1}}$.

Supporting Information

Are presented in the Supporting Information (Fig S1 to S6): the trajectory analysis of the reduced hPrx5 in the presence of 4NPC, the active site fluctuations observed during the simulations of Prx with ligands 4TBC and 4NPC, the histogram of the chemical shift perturbations (CSPs) induced by the binding of the different catechol derivatives with hPrx5, the IC50 determination for the 4NPC ligand, the Partial-Mixed Type Non Competitive Inhibition Model, the analysis of the inhibition mechanism assays realized on the 4NPC, and the ^{1}H and ^{13}C NMR spectra obtained for the synthesized compounds (intermediates and final product).
Abbreviations: CAT = catechol; 4MEC = 4-methylcatechol; 4TBC = 4-tertbutylcatechol; 4NPC = 4-neopentylcatechol; hPrx5 = Human Peroxiredoxin 5

Acknowledgements

We acknowledge la Région Rhônes Alpes for the grant no. 13-0118962-01 allocated to L.T. and J-M.L, and the Institut de Chimie de Lyon (2016) for the funding provided to all authors. We are grateful to Prof. B. Knoops and A. Clippe from the University of Louvain-la-Neuve, Belgium, for the generous gifts of biological materials to express and purify the recombinant proteins. We thank Acellera Company for providing a 6-month ACEMD multi-GPU software license and for the gift of a Nvidia Tesla K20 supercomputing unit. Finally, we thank Dr. Maggy Hologne for useful discussions and comments.

Competing Interests

The authors declare that they have no competing interests.

References

1. Hoffmann T.; Metternich R. The future of medicinal chemistry. *Angew.Chem. Int.*, 51:8670–8671, 2012.
2. Persch E.; Dumele O.; Diederich F. Molecular recognition in chemical and biological systems. *Angew.Chem. Int.*, 54:3290–3327, 2015.
3. Renaud J. P.; Neumann T.; Van Hijfte L. Fragment-based drug discovery. *Small Molecule Medicinal Chemistry: Strategies and Technologies*, 221, 2015.
4. Pan A. C.; Borhani D. W.; Dror R. O.; Shaw D. E. Molecular determinants of drug-receptor binding kinetics. *Drug Discov. Today*, 18:667–673, 2013.
5. Harvey M. J.; De Fabritiis G. High-throughput molecular dynamics: the powerful new tool for drug discovery. *Drug Discov. Today*, pages 1059–1062, 2012.
6. Harvey M. J.; Giupponi G.; Fabritiis G. Acemd: Accelerating biomolecular dynamics in the microsecond time scale. *J. Chem. Theory Comput.*, 5:1632–1639, 2009.
7. Barducci A.; Bussi G.; Parrinello M. Well-tempered metadynamics: A smoothly converging and tunable free-energy method. *Phys.Rev. Lett.*, 100, 2008.
8. Adcock S. A.; McCammon J. A. Molecular dynamics: Survey of methods for simulating the activity of proteins. *Chem. Rev.*, 106:1589–1615, 2006.
9. Joel José Montalvo-Acosta and Marco Cecchini. Computational Approaches to the Chemical Equilibrium Constant in Protein-ligand Binding. *Molecular Informatics*, 35(11-12):555–567, December 2016. ISSN 18681743. doi: 10.1002/minf.201600052.
10. Haohao Fu, Haochuan Chen, Marharyta Blazhynska, Emma Goulard Coderc de Lacam, Florence Szczepaniak, Anna Pavlova, Xueguang Shao, James C. Gumbart, François Dehez, Benoît Roux, Wensheng Cai, and Christophe Chipot. Accurate determination of protein:ligand standard binding free energies from molecular dynamics simulations. *Nature Protocols*, 17(4):1114–1141, April 2022. ISSN 1750-2799. doi: 10.1038/s41596-021-00676-1.
11. Darrin M. York. Modern Alchemical Free Energy Methods for Drug Discovery Explained. *ACS Physical Chemistry Au*, 3(6):478–491, October 2023. doi: 10.1021/acsphyschemau.3c00033.
12. James C. Gumbart, Benoît Roux, and Christophe Chipot. Standard Binding Free Energies from Computer Simulations: What Is the Best Strategy? *Journal of Chemical Theory and Computation*, 9(1):794–802, January 2013. ISSN 1549-9618. doi: 10.1021/ct3008099.
13. Alessandro Laio and Michele Parrinello. Escaping free-energy minima. *Proceedings of the National Academy of Sciences*, 99(20):12562–12566, October 2002. ISSN 0027-8424, 1091-6490. doi: 10.1073/pnas.202427399.
14. Giovanni Bussi and Alessandro Laio. Using metadynamics to explore complex free-energy landscapes. *Nature Reviews Physics*, pages 1–13, March 2020. ISSN 2522-5820. doi: 10.1038/s42254-020-0153-0.
15. Limongelli V.; Bonomi M.; Parrinello M. Funnel metadynamics as accurate binding free-energy method. *Proc. Natl. Acad. Sci. U.S.A.*, 110:6358–6363, 2013.
16. Troussicot L.; Guilliere F.; Limongelli V.; Walker O.; Lancelin J. M. Funnel-metadynamics and solution nmr to estimate protein-ligand affinities. *J. Am. Chem. Soc.*, 137:1273–1281, 2015.
17. Stefano Raniolo and Vittorio Limongelli. Ligand binding free-energy calculations with funnel metadynamics. *Nature Protocols*, 15(9):2837–2866, September 2020. ISSN 1750-2799. doi: 10.1038/s41596-020-0342-4.

18. Federica Moraca, Jussara Amato, Francesco Ortuso, Anna Artese, Bruno Pagano, Ettore Novellino, Stefano Alcaro, Michele Parrinello, and Vittorio Limongelli. Ligand binding to telomeric G-quadruplex DNA investigated by funnel-metadynamics simulations. *Proceedings of the National Academy of Sciences*, 114(11):E2136–E2145, March 2017. doi: 10.1073/pnas.1612627114.
19. Riccardo Capelli, Anna Bochicchio, GiovanniMaria Piccini, Rodrigo Casasnovas, Paolo Carloni, and Michele Parrinello. Chasing the full free energy landscape of neuroreceptor/ligand unbinding by metadynamics simulations. *Journal of Chemical Theory and Computation*, 15 (5):3354–3361, 2019.
20. Liu H. Yang K. Uncovering new conformational states of the substrate binding pocket of lsd1 potential for inhibitor design via funnel metadynamics. *J Phys Chem B.*, 128(1):137–149, 2024.
21. Knoops B.; Goemaere J.; Van der Eecken V.; Declercq J. P. Peroxiredoxin 5: structure, mechanism, and function of the mammalian atypical 2-cys peroxiredoxin. *Antioxidants redox signaling*, 15:817–829, 2011.
22. Portillo-Ledesma S.; Sardi F.; Manta B.; Tourn M. V.; Clippe A.; Knoops B.; Alvarez B.; Coitino E. L.; Ferrer-Sueta G. Deconstructing the catalytic efficiency of peroxiredoxin-5 peroxidatic cysteine. *Biochemistry*, 53:6113–6125, 2014.
23. Bernard Knoops, Vasiliki Argyropoulou, Sarah Becker, Laura Ferté, and Oksana Kuznetsova. Multiple Roles of Peroxiredoxins in Inflammation. *Molecules and Cells*, 39 (1):60–64, January 2016. ISSN 1016-8478. doi: 10.14348/molcells.2016.2341.
24. Arden Perkins, Kimberly J. Nelson, Derek Parsonage, Leslie B. Poole, and P. Andrew Karplus. Peroxiredoxins: Guardians against oxidative stress and modulators of peroxide signaling. *Trends in Biochemical Sciences*, 40(8):435–445, August 2015. ISSN 09680004. doi: 10.1016/j.tibs.2015.05.001.
25. Takashi Shichita, Eiichi Hasegawa, Akihiro Kimura, Rimpei Morita, Ryota Sakaguchi, Ichiro Takada, Takashi Sekiya, Hiroaki Ooboshi, Takanari Kitazono, Toru Yanagawa, Tetsuro Ishii, Hideo Takahashi, Shuji Mori, Masahiro Nishibori, Kazumichi Kuroda, Shizuo Akira, Kensuke Miyake, and Akihiko Yoshimura. Peroxiredoxin family proteins are key initiators of post-ischemic inflammation in the brain. *Nature Medicine*, 18(6):911–917, June 2012. ISSN 1546-170X. doi: 10.1038/nm.2749.
26. Sarah Barelier, Dominique Linard, Julien Pons, André Clippe, Bernard Knoops, Jean-Marc Lancelin, and Isabelle Krimm. Discovery of Fragment Molecules That Bind the Human Peroxiredoxin 5 Active Site. *PLOS ONE*, 5(3):e9744, March 2010. ISSN 1932-6203. doi: 10.1371/journal.pone.0009744.
27. Chow M. L.; Troussicot L.; Martin M.; Doumèche B.; Guillière F.; Lancelin J.-M. Predicting and understanding the enzymatic inhibition of human peroxiredoxin 5 by 4-substituted pyrocatechols combining funnel-metadynamics, solution nmr and steady-state kinetics. *Biochemistry*, 55:3469–3480, 2016.
28. Massimiliano Bonomi, Alessandro Barducci, and Michele Parrinello. Reconstructing the equilibrium Boltzmann distribution from well-tempered metadynamics. *Journal of Computational Chemistry*, 30(11):1615–1621, August 2009. ISSN 01928651, 1096987X. doi: 10.1002/jcc.21305.
29. Bonomi M.; Branduardi D.; Bussi G.; Camilloni C.; Provasi D.; Raiteri P.; Donadio D.; Marinelli F.; Pietrucci F.; Broglia R. A.; Parrinello M. Plumed: A portable plugin for free-energy calculations with molecular dynamics. *Comput. Phys. Commun.*, 180:1961–1972, 2009.
30. Kuzmič P. Program dynafit for the analysis of enzyme kinetic data: application to hiv proteinase. *Anal Biochem.*, 237(2):260–73, 1996.
31. Kuzmič P. Dynafit–a software package for enzymology. *Methods Enzymol.*, 467:247–280, 2009.
32. Declercq J. P.; Evrard C.; Clippe A.; Stricht D. V.; Bernard A.; Knoops B. Crystal structure of human peroxiredoxin 5, a novel type of mammalian peroxiredoxin at 1.5 a resolution. *J.Mol.Biol*, 311:751–759, 2001.
33. Hall A.; Parsonage D.; Poole L. B.; Karplus P. A. Structural evidence that peroxiredoxin catalytic power is based on transition-state stabilization. *J.Mol.Biol.*, 402:194–209, 2010.
34. Brice M. D.; Rodgers J. R.; Kennard O.; Shimanouchi T.; Tasumi M. Bernstein F. C.; Koetzle T. F.; Williams G. J.; Meyer E. F. The protein data bank: a computer-based archival file for macromolecular structures. *Arch.Biochem.Biophys.*, 185:584–591, 1978.
35. Cornell W. D.; Cieplak P.; Bayly C. I.; Gould I. R.; Merz K. M.; Ferguson D. M.; Spellmeyer D. C.; Fox T.; Caldwell J. W.; Kollman P. A. A second generation force field for the simulation of proteins, nucleic acids, and organic molecules. *J. Am. Chem. Soc.*, 117:5179–5197, 1995.
36. Hornak V.; Abel R.; Okur A.; Strockbine B.; Roitberg A.; Simmerling C. Comparison of multiple amber force fields and development of improved protein backbone parameters. *Proteins*, 65:712–725, 2006.
37. Lindorff-Larsen K.; Piana S.; Palmo K.; Maragakis P.; Klepeis J. L.; Dror R. O.; Shaw D. E. Improved side-chain torsion potentials for the amber ff99sb protein force field. *Proteins*, 78: 1950–1958, 2010.
38. Jorgensen W. L.; Madura J. D. Quantum and statistical mechanical studies of liquids : Solvation and conformation of methanol in water. *J. Am. Chem. Soc.*, 105:1407–1413, 1983.
39. Wang J.; Wolf R. M.; Caldwell J. W.; Kollman P. A.; Case D. A. Development and testing of a general amber force field. *J. Comput. Chem.*, 25:1157–1174, 2004.
40. Wang J.; Wang W.; Kollman P. A.; Case D. A. Automatic atom type and bond type perception in molecular mechanical calculations. *J. Mol. Graph. Model*, 25:247–260, 2006.
41. Dalke A. Humphrey W. and Schulten K. Vmd: visual molecular dynamics. *J. Molec. Graphics*, 14:33–38, 1996.
42. Laurie J. Heyer, Semyon Kruglyak, and Shibu Yooseph. Exploring Expression Data: Identification and Analysis of Coexpressed Genes. *Genome Research*, 9(11):1106–1115, January 1999. ISSN 1088-9051, 1549-5469. doi: 10.1101/gr.9.11.1106.
43. Tran P. H.; Duus F.; Le T. N. Friedel–crafts acylation using bismuth triflate in [bmi][pf6]. *Tetrahedron Lett.*, 53:222–224, 2012.
44. Guyon C.; Baron M.; Lemaire M.; Popowycz F.; Métay E. Commutative reduction of aromatic ketones to arylmethylenes/alcohols by hypophosphites catalyzed by pd/c under biphasic conditions. *Tetrahedron*, 70:2088–2095, 2014.
45. A. Delaglio F.; Grzesiek S.; Vuister G. W.; Zhu G.; Pfeifer, J.; Bax. Nmrpipe: a multidimensional spectral processing system based on unix pipes. *J. Biomol. NMR*, 6:277–293, 1995.
46. Johnson B.; Blevins R. Nmr view: A computer program for the visualization and analysis of nmr data. *J. Biomol. NMR*, 4:603–614, 1994.
47. O. Lange A.; Hoeller D.; Wienk H.; Marcillat O.; Lancelin, J. M.; Walker. Nmr reveals a different mode of binding of the stam2 vhs domain to ubiquitin and diubiquitin. *Biochemistry*, 50:48–62, 2011.